Eur. Phys. J. D **22**, 53–64 (2003)
DOI: 10.1140/epjd/e2002-00222-0

THE EUROPEAN PHYSICAL JOURNAL D

From direct to absolute mass measurements: A study of the accuracy of ISOLTRAP

A. Kellerbauer[1,a], K. Blaum[2], G. Bollen[3], F. Herfurth[1], H.-J. Kluge[2], M. Kuckein[4], E. Sauvan[1,b], C. Scheidenberger[2], and L. Schweikhard[5]

[1] CERN, Division EP, 1211 Genève 23, Switzerland
[2] GSI, Planckstr. 1, 64291 Darmstadt, Germany
[3] NSCL, Michigan State University, East Lansing, MI 48824, USA
[4] Inst. f. Physik, Technische Universität München, 85748 Garching, Germany
[5] Inst. f. Physik, Ernst-Moritz-Arndt-Universität Greifswald, 17487 Greifswald, Germany

Received 7 June 2002
Published online 6 November 2002 –

Abstract. For a detailed study of the accuracy of the Penning trap mass spectrometer ISOLTRAP all expected sources of uncertainty were investigated with respect to their contributions to the uncertainty of the final result. In the course of these investigations, cross-reference measurements with singly charged carbon clusters $^{12}C_n^+$ were carried out. The carbon cluster ions were produced by use of laser-induced desorption, fragmentation, and ionization of C_{60} fullerenes and injected into and stored in the Penning trap system. The comparison of the cyclotron frequencies of different carbon clusters has provided detailed insight into the residual systematic uncertainty of ISOLTRAP and yielded a value of 8×10^{-9}. This also represents the current limit of mass accuracy of the apparatus. Since the unified atomic mass unit is defined as 1/12 of the mass of the ^{12}C atom, it will be possible to carry out absolute mass measurements with ISOLTRAP in the future.

PACS. 07.75.+h Mass spectrometers – 21.10.Dr Binding energies and masses – 32.10.Bi Atomic masses, mass spectra, abundances, and isotopes – 36.40.Wa Charged clusters

1 Introduction

1.1 The ISOLTRAP experiment

The ISOLTRAP experiment is a Penning trap mass spectrometer for accurate high-precision measurements of atomic masses. It is installed at the on-line isotope separator ISOLDE at CERN (Geneva, Switzerland) [1], and it is mainly intended for mass measurements of short-lived radioactive nuclides. The masses of close to two hundred radionuclides have already been measured with the ISOLTRAP apparatus [2].

ISOLTRAP consists of a radiofrequency quadrupole (RFQ) ion beam cooler and buncher [3] and two Penning traps, each located in the field of a superconducting magnet [4]. The RFQ ion beam cooler and buncher (RICB) serves the purpose of decelerating, accumulating, cooling, and bunching the 60-keV ISOLDE ion beam. The first Penning trap is a cylindrical trap which is used for the cooling and isobaric cleaning of the ion bunches. The actual mass measurement is carried out in the second Penning trap, a hyperboloidal trap. It is based on a determination of the cyclotron frequency ν_c of an ion with charge q and unknown mass m_{ion} in a magnetic field of magnitude B [4]:

$$\nu_c = \frac{1}{2\pi}\frac{qB}{m_{ion}} \cdot \tag{1}$$

The cyclotron frequency is measured *via* the resonant excitation of an ion's characteristic radial motions in a Penning trap [5,6].

In order to deduce the mass m_{ion} from its cyclotron frequency ν_c by use of equation (1), the magnitude of the magnetic field in the trap must be known accurately. This is achieved by measuring the cyclotron frequency of a stable ion with well-known mass, the so-called reference ion.

1.2 Pushing the limits of mass accuracy

Penning traps are the most precise tools for direct mass measurements available today. This fact has most recently been demonstrated by measurements of the mass of the

[a] e-mail: a.kellerbauer@cern.ch
[b] *Current address*: Centre de Physique des Particules de Marseille, 13288 Marseille Cedex 9, France.

electron with the Penning trap mass spectrometer at the University of Washington [7], by a determination of the charge-to-mass ratios of the proton and the antiproton with the TRAP apparatus at CERN [8], and by mass measurements on hydrogen and helium with the Penning trap setup at the University of Mainz [9].

More particularly in the field of heavy-ion spectrometry, recent mass measurements of stable nuclides with the SMILETRAP apparatus [10] and with the Penning trap at MIT [11] have shown that Penning trap mass spectrometry can reach relative uncertainties of a few parts in 10^{-10} or better. SMILETRAP is connected to an electron beam ion source which supplies it with highly charged stable ions. As can be seen from equation (1), the higher charge state leads to a higher cyclotron frequency and thus, for a given frequency precision, to a smaller relative uncertainty. The performance of the MIT Penning trap is reached by placing the trap inside the cold bore of a superconducting magnet. This assures temperature stability of the trap and surrounding material as well as an ultra-high vacuum, thereby allowing long observation times (many hours) of single ions.

Radioactive nuclides, however, with their low production rates and short half-lives, as well as the environment necessary to create them, represent difficult challenges for a high-precision measurement in this field. ISOLTRAP is the apparatus that allows the most precise direct mass measurements of radioactive nuclides today.

There has been growing motivation for pushing the limits of the precision of mass measurements of radioactive nuclides beyond 10^{-7}. Fundamental studies for instance, such as a verification of the conservation of the weak vector current (CVC hypothesis) or the unitarity of the Cabbibo-Kabayashi-Maskawa (CKM) matrix, both postulates of the standard model, require accurate mass measurements with precisions at the 10^{-8} level [12]. Also, the binding energies of halo nuclides or nuclides at shell closures are of special interest and require high mass precision.

In the past, the uncertainty of ISOLTRAP mass measurements due to all known or expected systematic effects was taken into account by the addition of a relative uncertainty to the final result. Based on an earlier study of the contributing effects, the magnitude of this relative uncertainty was conservatively estimated to be 10^{-7} [4]. This included fluctuations of the magnetic field during the measurement as well as possible imperfections of the magnetic and electric fields. Even in the cases where production rates were high or where a large number of measurements could be conducted, the relative uncertainty of the final result was therefore limited to 10^{-7}.

Typical reference ions used in ISOLTRAP mass measurements are ^{39}K, ^{85}Rb, ^{87}Rb, and ^{133}Cs. These four nuclides can be produced in the surface ionization ion source that is mounted upstream of the ISOLTRAP triple trap setup. Except for ^{39}K, their masses have been measured with relative uncertainties at the 10^{-10} level [11]. However, for measurements of nuclides whose mass falls outside of the range spanned by these four nuclides or differs by many mass units from the mass of the one nearest to it, an ion that is also produced by ISOLDE must be chosen. The masses of these reference ions are often not known to high precision. This insufficient knowledge of the mass of the reference ion is an additional source of uncertainty when the final result is to be expressed in terms of mass.

The main aim of the present study was to attempt to identify and quantify all effects that contribute to the uncertainty of the primary result. A special emphasis was placed on identifying effects whose importance can be diminished by conducting a larger number of measurements. The ideal test bed for these tests was found in the carbon clusters, which can be readily produced from the fragmentation of C_{60} fullerenes, the ball-shaped molecules of carbon.

1.3 Carbon clusters

The discovery and synthesis of C_{60} and C_{70} [13,14] has stimulated exciting scientific studies. The fact that C_{60} fullerenes can now be produced in macroscopic amounts and with high purity has opened the way for a variety of technical developments and fundamental research [15,16]. Ionized carbon clusters produced *via* laser-induced fragmentation and ionization of C_{60} can now also be readily studied in ISOLTRAP's tandem Penning trap setup [17,18].

Apart from the molecular binding energies, all carbon clusters that are composed solely of the most abundant isotope ^{12}C have masses that are exact multiples of the unified atomic mass unit u [19]. They would therefore be the ideal choice of reference ions. This would allow to perform absolute mass measurements with ISOLTRAP, *i.e.* mass measurements in which the reference ion has no mass uncertainty. In this case, ISOLTRAP's final result could directly be expressed as a mass in atomic mass units.

Since carbon clusters with a wide range of masses and a mass spacing of only 12 u can be produced, they also constitute a dense grid for the investigation of systematic effects. In a cross-reference mass measurement, a measurement which is carried out using carbon clusters both as the reference ion and as the ion of interest, the true value of the ratio of the cyclotron frequencies $\nu_{c,ref}/\nu_c$ is exactly known. This means that cross-reference measurements can be used to identify errors of the apparatus or the measurement procedure and that the knowledge obtained in this way can be used to determine the uncertainties of actual mass measurements.

We have conducted a large number of these cross-reference measurements to verify the validity of a redefined measurement and analysis procedure. As a whole, they provide detailed information on the relative combined standard uncertainty $u_c(r)/r$ of a cyclotron frequency ratio determination. A χ^2 test of that distribution gives insight into the possible presence and magnitude of residual systematic effects beyond those already taken into account in the new analysis procedure.

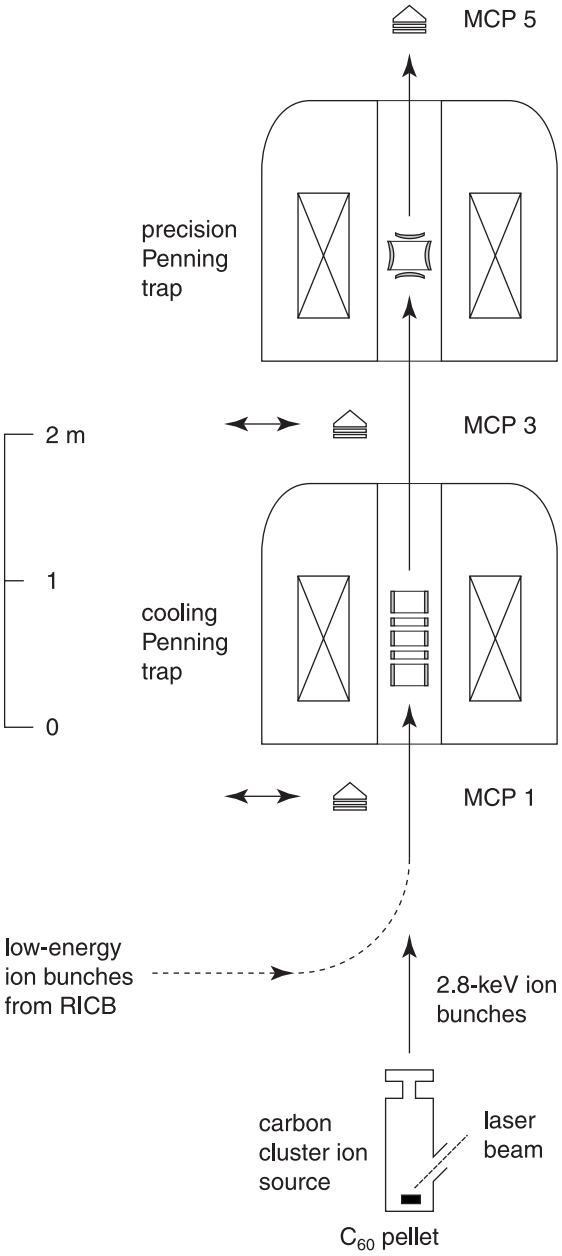

Fig. 1. Overview sketch of the ISOLTRAP setup with the carbon cluster ion source. The source is mounted about 2 m below the cooling Penning trap.

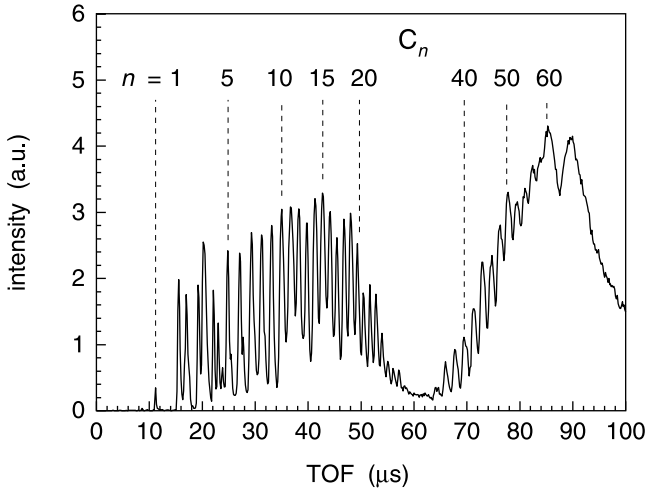

Fig. 2. Time-of-flight mass spectrum of carbon cluster ions produced by use of laser-induced desorption, fragmentation, and ionization of C_{60} at 532 nm at a laser pulse energy of about 10 mJ, recorded at MCP 1 [17]. The peak around $n = 70$ is probably due to coalescence products of C_{60} and smaller fragments.

2 Experimental setup and procedure

2.1 Carbon cluster ion source

The carbon cluster ion source is mounted about 2 m below the cooling Penning trap. Figure 1 shows an overview sketch of ISOLTRAP's tandem Penning trap setup with the carbon cluster source.

The carbon cluster ions are produced by use of laser-induced desorption, fragmentation, and ionization of C_{60} fullerenes. To this end, the frequency-doubled beam of a Q-switched Nd:YAG laser (Quantel Brilliant B; repetition rate 1–10 Hz; pulse duration 6 ns; frequency 532 nm) is focused on a C_{60} pellet (Aventis; purity of $C_{60} > 99\%$), which is placed at an accelerating potential of 2.8 kV. The focal spot area of the laser is about 0.1 mm^2 with a typical pulse energy of 10 mJ at 532 nm, corresponding to an estimated fluence of 10 J/cm^2. Desorption and ionization of C_{60} set in at a laser pulse energy of about 5 mJ. At slightly higher pulse energies, the intensity of C_{60}^+ increases strongly and small amounts of lighter carbon cluster ions are produced by fragmentation [20].

The charged fullerene fragments C_n^+ are then electrostatically accelerated to 2.8 keV and transferred towards the cooling Penning trap. A typical time-of-flight (TOF) mass spectrum is shown in Figure 2. It was recorded on the micro-channel-plate (MCP) detector MCP 1 at a laser pulse energy of 10 mJ. The spectrum is characterized by a strong production of the high-mass, even-numbered fragments (fullerene fragments C_{34-58}^+) and low-mass fragments C_n^+, $n \leq 27$. Between these two regions, a gap is observed. These characteristics of the spectrum are experimentally well understood in terms of the geometrical properties of the clusters [21]. Coalescence products of C_{60} and smaller fragments are observed in the spectrum beyond $n > 60$.

Ion beams that are produced either at the ISOLDE target–ion source combination or at the surface ionization reference source pass through the RICB, where they are radially confined in an RFQ field and cooled in buffer gas collisions. In a region towards the end of the RICB, they are longitudinally confined before being ejected towards the cooling Penning trap in bunches [3].

Carbon clusters that are produced in the carbon cluster laser ion source are directly transferred to the cooling Penning trap. In the current setup, ions from ISOLDE and from the cluster source cannot be used simultaneously for mechanical reasons.

2.2 Penning trap setup

In a Penning trap, the motion of an ion is the superposition of three harmonic motions, one axial and two radial. The two radial motions, the magnetron motion with frequency ν_- and the cyclotron motion with reduced frequency ν_+, can be coupled by an azimuthal quadrupolar excitation at the sum frequency. The sum frequency is in fact the cyclotron frequency ν_c of an ion in a pure magnetic field [22]:

$$\nu_c = \nu_+ + \nu_- . \tag{2}$$

This behavior is exploited in both Penning traps of the ISOLTRAP setup.

In the buffer-gas-filled cooling trap, all three characteristic motions of the ions are cooled in buffer gas collisions. A cooling of the magnetron motion, however, leads to an increase of its radius. The radial motions of the ions can be excited by means of an azimuthal quadrupolar RF field applied to the segmented ring electrode of the trap. When the ions are excited at the sum frequency of the two characteristic radial motions, these motions are coupled and the magnetron motion is constantly converted into cyclotron motion, which in turn is cooled away. This cooling and centering technique is mass-selective and therefore can be used for an isobaric cleaning of the ion sample [23]. Storage times of several hundred milliseconds without significant losses are achieved in the cooling trap. Typical mass resolving powers are of the order of 10^4 to 10^5 [4].

The selected ion species is then transferred to the precision Penning trap. The precision trap also has a segmented ring electrode, but instead of containing a buffer gas, it is operated at high vacuum. After the transfer from the cooling trap, the ions are first subjected to an azimuthal dipole excitation at the magnetron frequency which causes an increase of the magnetron radius. An azimuthal quadrupolar RF field at the sum frequency of the two characteristic radial motions then leads to a conversion of the magnetron motion into cyclotron motion. Since the reduced cyclotron frequency is much larger than the magnetron frequency, the ions gather kinetic energy in the process. When the ion bunch is finally ejected out of the trap towards an MCP detector, the radial energy is converted into longitudinal energy as the ions pass through the inhomogeneous-magnetic-field region of the superconducting magnet. Therefore, the ions whose radial motion has been resonantly excited reach the detector after a reduced flight time compared to those whose magnetron motion has not been converted into cyclotron motion [5,6].

The frequency of the azimuthal quadrupolar excitation is scanned, leading to a TOF resonance, of which a typical example for C_9^+ ions is shown in Figure 3. The shape of this resonance is well understood [24] and its functional representation can be used to perform a least-squares fit to the data points and extract the cyclotron frequency of the ion and its experimental standard deviation.

The TOF uncertainty of the data points in a resonance such as that shown in Figure 3 is mainly due to the random

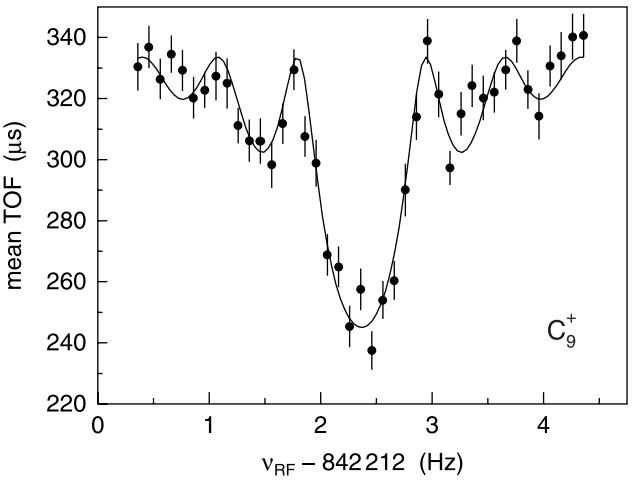

Fig. 3. Time-of-flight resonance curve of C_9^+. The solid line is a fit of the expected line shape to the data points [24]. The reduced χ^2 of the least-squares fit of the complete resonance is close to one.

distribution of the axial energy of the ions in the precision trap before they are ejected. The uncertainty of the time of flight at a given excitation frequency ν_{RF} is assigned as a function of the width of the TOF distribution and the number of detected ions for that frequency. In all records with a sufficient number of detected ions, the reduced χ^2 of the fit is close to one.

2.3 Principle of a mass measurement

Assuming that all ion species have the same charge $q = +e$, the atomic mass m of the ion of interest can be calculated from the cyclotron frequency[1] of the reference ion ν_{ref}, the cyclotron frequency of the ion of interest ν, the atomic mass of the reference ion m_{ref}, and the electron mass m_e:

$$m = \frac{\nu_{ref}}{\nu}\,(m_{ref} - m_e) + m_e . \tag{3}$$

However, in this manner, the uncertainty of the atomic mass of the reference ion contributes to the uncertainty of the mass result as well.

That is why ISOLTRAP's results are always also reported in terms of the ratio r of the cyclotron frequencies:

$$r = \frac{\nu_{ref}}{\nu} . \tag{4}$$

In this way, the mass of the ion of interest can be obtained at any given time using the most up-to-date knowledge of the mass of the reference ion. The primary result is independent of any changes in that knowledge.

The more rapidly obtained reference measurement is made before and after that of the ion of interest.

[1] In the following, the cyclotron frequency ν_c will be denoted by the symbol ν to simplify the notation.

The measured cyclotron frequency determinations are later interpolated to the time of the measurement of the ion of interest.

A complete ISOLTRAP mass measurement thus consists of three separate cyclotron frequency determinations: that of the ion of interest, preceded and followed by that of the reference ion. The measurand is their cyclotron frequency ratio r. The combined standard uncertainty of the final result is determined by the experimental standard deviations of the frequency measurements according to the law of propagation of uncertainty as well as by the various uncertainties due to systematic effects in the measurement procedure.

3 Uncertainties of the measured quantities

In this section, all identified effects that contribute to the uncertainty of the primary result, the mean cyclotron frequency ratio $\bar{r}$, are discussed. For the sake of consistency, relative uncertainties are used throughout.

3.1 Cyclotron frequency of the ion of interest

3.1.1 Statistical uncertainty

For any recorded TOF resonance, the experimental standard deviation $s(\nu)$ of the cyclotron frequency ν is a function of the resolving power of the precision trap, *i.e.* the RF excitation time T_{RF}, and the total number N_{tot} of ions recorded. An empirical formula for this relation has been proposed [2]:

$$\frac{s(\nu)}{\nu} = \frac{1}{\nu}\frac{c}{\sqrt{N_{\mathrm{tot}}}T_{\mathrm{RF}}}\,, \tag{5}$$

where c is expected to be a dimensionless constant.

In a series of cyclotron frequency measurements of the nuclide ^{85}Rb, the functional relation proposed in equation (5) was verified and c determined. Figure 4 shows the result of these measurements for different excitation times T_{RF} as a function of the number of ions N_{tot} recorded in a TOF resonance. To obtain records with different numbers of ions, long measurements were subdivided into several parts. It is found that c is in fact independent of the excitation time and the number of ions, with an average value of

$$c = 0.898(8). \tag{6}$$

In measurements with a very low total number of ions (less than about 300), it has been observed that c is smaller than the value found for standard measurements. The reasons for this deviation are not yet well understood. In the presence of contaminations, a larger total number of ions must be accumulated to achieve a given statistical uncertainty and c is therefore larger than the standard value found above.

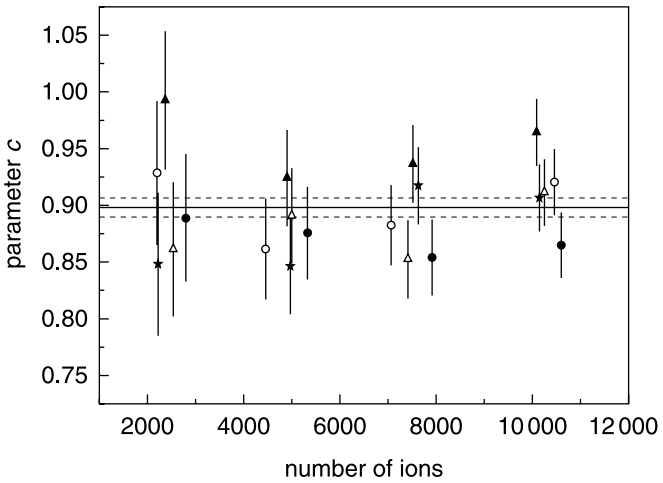

Fig. 4. Determination of the parameter c of equation (5) from a series of cyclotron frequency measurements of $^{85}Rb^{+}$. The parameter is plotted as a function of the number of ions N_{tot} recorded in a TOF resonance. The data labels represent different RF excitation times T_{RF}: 300 ms (empty circles), 600 ms (filled circles), 900 ms (empty triangles), 1200 ms (filled triangles), and 1500 ms (stars). The solid horizontal line is the weighted mean of all values and the dashed lines show the 1σ confidence interval of the mean.

3.1.2 Contaminations

The reference ions are produced in a dedicated ion source which makes available the ions of a few surface-ionizable elements. The mass separation between these species is sufficient to prevent mutual contaminations from reaching the precision trap. No contaminations stemming from the reference ion source have until now been observed in the precision Penning trap.

In the case of the ions of stable or radioactive nuclides produced in the ion source of the ISOLDE target, however, the presence of contaminations has to be expected. These can be isobaric or isomeric impurities that originate in the target or ion source itself, contaminations that are produced in the ISOLTRAP apparatus through charge exchange reactions with the buffer gas or with rest gas, or decay products of short-lived radioactive ions. Doubly charged ions undergo charge exchange reactions in the RICB where their charge state is either reduced to one or they are neutralized. Charge states higher than one have not been observed beyond the cooler and buncher stage.

The effect of the presence of a contaminant ion in the precision Penning trap has been extensively studied [24,25]. For a low number of ions in the precision trap, it expresses itself by the appearance of two separate resonance curves (assuming sufficient resolving power), one of which can be outside of the scanning range of the quadrupolar-excitation frequency. As the ion number in the trap increases, these two resonance peaks successively approach each other. At the same time, the centroids are shifted to lower frequencies.

In order to correct for this contamination shift, ν is determined for different count rate classes, *i.e.* for different

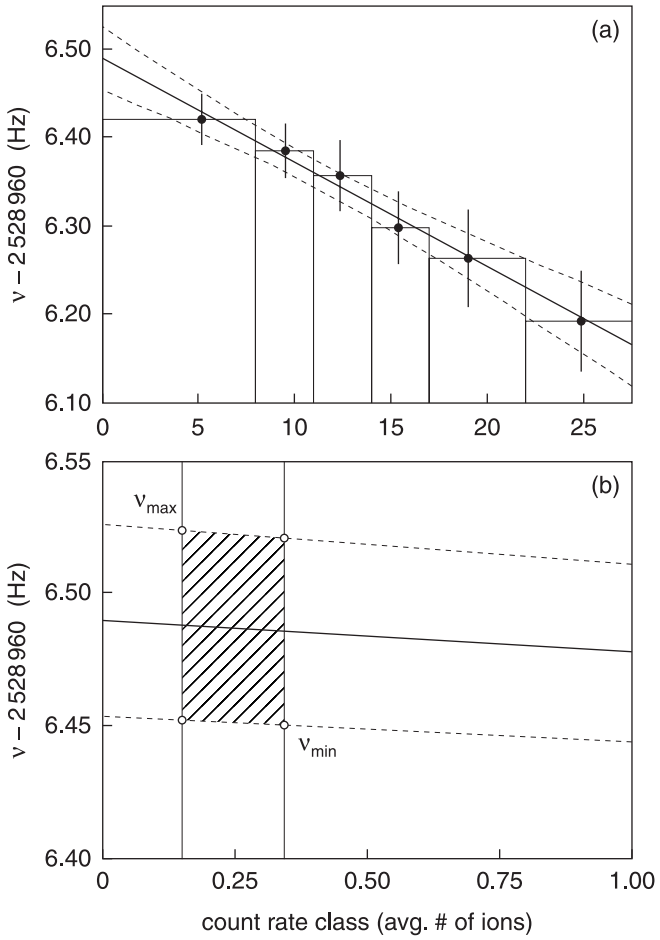

Fig. 5. (a) Count rate dependence of the observed cyclotron frequency. The measurement was made with $^{36}Ar^{+}$ ions from ISOLDE, the contamination is probably due to $^{36}Cl^{+}$ ions. The count rate classes are indicated by the bins. The straight line is a linear least-squares fit to the data points, the dashed lines are the 1-sigma confidence bands of the fit. (b) Detail for the extrapolation into the count rate class region between 0 and 1. The two vertical lines enclose the estimated micro-channel-plate detector efficiency of $\epsilon = 0.25(10)$. The labeled points represent the upper and lower bounds of the extrapolated cyclotron frequency.

numbers of ions that were present in the precision trap. The centroid frequencies are plotted as a function of the center of gravity of the count rate distribution in that class. An example of such a plot for $^{36}Ar^{+}$ is shown in Figure 5a. A linear least-squares fit is then applied to the data points, shown as the solid straight line in the figure. The dashed lines represent the 1σ confidence interval of the fit, which in this case is of the order of 10^{-8} in relative uncertainty.

If the detection efficiency ϵ of the MCP detector of the precision Penning trap were unity, a linear extrapolation of these data points to ion number unity would then yield the corrected centroid frequency. In reality, the detection efficiency of an MCP detector at an ion energy of about 1 keV is estimated to be only $\epsilon = 0.25(10)$ [26]. This means that when a single ion is observed in the trap, about four ions were actually present on average. Therefore, the linear fit must be extrapolated beyond unity.

Figure 5b shows how the extrapolated cyclotron frequency and its uncertainty are obtained from the fit. The open points represent the upper and lower bounds $\nu_{\max}$ and $\nu_{\min}$ of the extrapolated cyclotron frequency. The corrected frequency and its uncertainty are then calculated from

$$\nu = \frac{\nu_{\max} + \nu_{\min}}{2} \tag{7}$$

and

$$s(\nu) = \frac{\nu_{\max} - \nu_{\min}}{2}\,, \tag{8}$$

which for the example of Figure 5 results in a relative uncertainty of $s(\nu)/\nu = 1.5 \times 10^{-8}$.

3.2 Cyclotron frequency of the reference ion

The magnitude of the magnetic field in the precision Penning trap varies with time. The following mechanisms for a change in the magnetic-field magnitude of a superconducting magnet have been identified:

1. the current in the superconducting coils of the magnet decreases steadily due to a phenomenon called flux creep [27,28]. It occurs when flux lines, which are pinned to inhomogeneities of the superconducting material, jump from one pinning site to another. The decrease of the field due to the viscous drag force that results from this phenomenon follows a logarithmic decay of the form $[1 - d\ln(t/\tau_0)]$, where d and τ_0 are phenomenological parameters [29]. Over short time intervals (up to years), this logarithmic decay can be approximated by a linear decrease;
2. when objects containing ferromagnetic or paramagnetic materials are brought within a short distance of a few meters or less of the magnet, they are magnetized. This magnetization distorts the field of the magnet. For large metallic objects such as the crane in the ISOLDE hall, the resulting field jumps can be of the order of 10^{-7}. This effect is easily avoided during measurements by locking the crane in a remote location of the hall and otherwise avoiding to handle ferromagnetic or paramagnetic objects near the magnets;
3. the pressure on the recovery line for evaporated gaseous helium is subject to fluctuations. This directly determines the boiling point of the liquid helium and thus influences its temperature and that of all materials in direct contact with it, including insulator material in the high-magnetic-field region. The temperature dependence of the magnetic permeability of these materials then causes fluctuations in the magnitude of the magnetic field inside the trap [30];
4. the temperature in the warm bore of the superconducting magnet fluctuates with the temperature of the experimental hall. The magnetic permeability of all

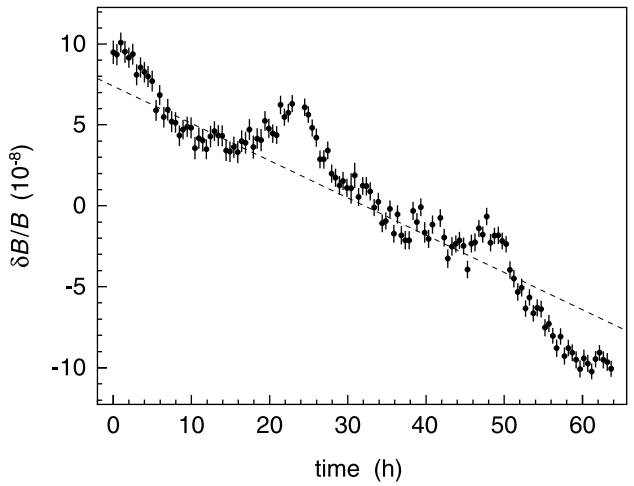

Fig. 6. Relative change of the magnetic-field magnitude in the precision trap over a time of more than 60 hours. Both the steady decrease and the superimposed random fluctuations can be observed. The measured slope of the slow decay given by equation (9) is indicated by the dashed line.

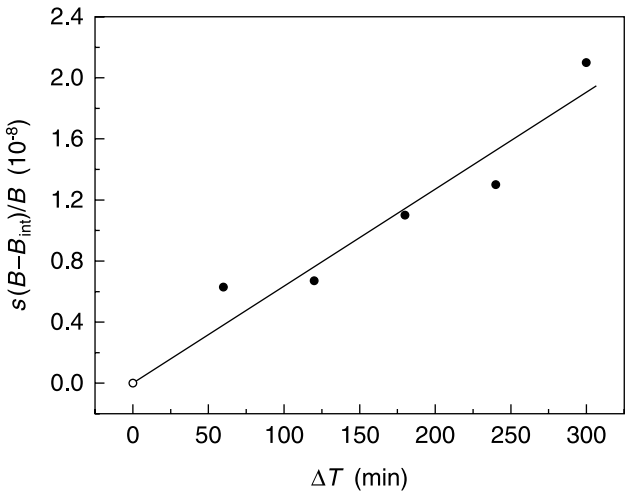

Fig. 7. Relative standard deviation of the magnetic-field magnitude B about the interpolated value $B_{\rm int}$ for different time intervals ΔT between the two reference measurements, obtained *via* cyclotron frequency measurements of $^{85}Rb^{+}$. Since the data points represent the standard deviation of a measured quantity, they cannot be assigned an uncertainty (error bar).

materials surrounding the Penning trap, such as the stainless-steel vacuum chamber, varies with temperature as well, and this also has an effect on the magnetic-field magnitude.

An effort to stabilize both the temperature in the warm bore and the pressure in the helium Dewar vessel of the SMILETRAP setup has proven successful in reducing the short-term magnetic-field fluctuations [31]. In the case of the magnet of ISOLTRAP's precision trap, the total relative field decay has been measured over a period of about 40 days to be

$$\frac{\delta B}{\delta t}\frac{1}{B} = -2.30(3) \times 10^{-8}/\mathrm{h}\,. \qquad (9)$$

Figure 6 shows the relative change in the magnetic-field magnitude in the precision trap over an interval of more than 60 hours. The data were obtained by a continuous measurement of the cyclotron frequency of one single species of ions, in this case $^{85}Rb^{+}$. Both the long-term trend and the short-term fluctuations can be observed. It can be seen that the random fluctuations are of the same order of magnitude as the steady decay. In this run as well as in some others, there appears to be a 24-hour periodicity in the short-term fluctuations which can be explained by day–night temperature changes in the ISOLDE hall. This effect is, however, not regular enough to allow it to be corrected for. It must be taken into account by the addition of an uncertainty.

Because of the time dependence of the magnetic field, the cyclotron frequencies of the two ions should be measured in as short an interval as possible. Therefore, one reference measurement is carried out just before and one just after the actual measurement. The cyclotron frequency of the reference ion is then interpolated to the time of the actual measurement. The linear interpolation represents a weighted mean that gives a stronger weight to the reference that is closer to the measurement of the ion of interest. On average, it also takes into account the slow decay of the magnetic field. The reliability of this interpolation obviously decreases with the time that elapses between the two reference measurements. This additional uncertainty, which must be added to the confidence interval of the interpolation, corresponds to the erratic component of the magnetic-field change.

In order to determine the deviation of the magnetic field from the linear decrease, we have conducted a series of long-term measurements such as the one shown in Figure 6. In these tests, care was taken to accumulate a maximum of statistics by using a fairly high number of ions in the trap at a time ($\approx$ 20 counts). For the analysis, the data files were later subdivided into segments that simulate complete measurements consisting of two references and one simulated measurement of the ion of interest. The deviation of the measured cyclotron frequency from the expected value obtained from the linear interpolation of the two simulated reference measurements is then a measure for the non-linearity of the magnetic-field drift.

The relative standard deviation $s(B - B_{\rm int})/B$ of the magnetic-field magnitude B about the interpolated value $B_{\rm int}$ as a function of the time ΔT elapsed between the two reference measurements[2] is shown in Figure 7. For reasons of simplicity, the duration of each of the reference measurements was always chosen to be about 15 minutes, which is the typical duration of reference measurements in on-line experiments. The data points agree well with a fitted straight line that by definition has to go through the

[2] ΔT is understood to mean the time difference between the centers of the two measurements. The definition is chosen in this way in order to allow the linear fit of the data to be constrained to pass through the origin.

origin. The fit yields the slope of the linear time dependence of the standard deviation. Because of the proportionality of B and ν for an ion with given mass and charge that follows from equation (1), this same time dependence also governs the standard uncertainty $u_B(\nu_{\rm ref})/\nu_{\rm ref}$ of the cyclotron frequency of the reference ion due to magnetic-field fluctuations:

$$\frac{u_B(\nu_{\rm ref})}{\nu_{\rm ref}} = 6.35(45) \times 10^{-11}/\text{min} \times \Delta T. \qquad (10)$$

This result bears as a consequence for high-precision mass measurements that the total duration of the measurement must be kept as short as possible. In experiments using radionuclides whose production rates are very low, the time required for collecting sufficient statistics for a cyclotron frequency determination can in some cases be as long as several hours. In those instances, a comparatively large uncertainty contribution due to magnetic-field fluctuations can be avoided by interrupting the on-line measurement and quickly obtaining a reference.

3.3 Cyclotron frequency ratio

3.3.1 Cross-reference measurements

Over a time of about three months, more than one hundred cross-reference measurements with carbon clusters were conducted with ISOLTRAP. In three series of measurements, the singly charged ions of C_{10}, C_{12}, and C_{20} were in turn used as reference ions. All singly charged carbon clusters $^{12}C_n^+$ with $6 \leq n \leq 20$ were used as simulated ions of interest. The ion-optical elements along the path of the carbon cluster ions were optimized to a mass of about 100 u at the beginning of this study. This, together with low production rates (as seen in Fig. 2), caused the count rates of clusters with $n < 6$ and $n > 20$ to be too low for cyclotron frequency determinations within a reasonable amount of time. This is not a principal limitation of the apparatus, however, and can be adjusted in future experiments.

For each individual TOF resonance, about 3 000 counts were recorded. The duration of the quadrupolar excitation was varied between 900 ms and 3 s, corresponding to resolving powers between 6×10^5 and 3×10^6; the relative statistical uncertainty $s(\nu)/\nu$ in the determination of the cyclotron frequency was a few 10^{-8} for each single measurement. Depending on the production rates and the excitation times, each resonance took between 15 min and 3 h. A count rate dependence of the cyclotron frequency determination was not observed with carbon clusters. This indicates that all isobaric contaminant ions as well as clusters containing the second most abundant isotope ^{13}C were successfully removed in the cooling trap.

The molecular binding energies of the carbon clusters, which are of the order of $|V_{\rm b}|/(mc^2) \approx 10^{-9}$, cannot be entirely neglected in a high-precision study. However, theoretical calculations suggest a smooth behavior of the binding energies with magnitudes between 5.6 and 7 eV per atom for the clusters C_n with $6 \leq n \leq 20$ [32,33]. Therefore, under the assumption that the molecular binding energy *per atom* is approximately constant, its contribution to the cluster ion mass cancels out in the calculation of a cyclotron frequency ratio.

For each individual measurement, the standard uncertainty $u(r)$ of the measured cyclotron frequency ratio, including the uncertainty due to magnetic-field fluctuations according to equation (10), and its deviation $\varepsilon(r) = r - r_{\rm th}$ from the true value were determined. Figure 8 shows the result of the 114 measurements in the form of ideograms. An ideogram is obtained by associating with each individual measurement a Gaussian distribution whose width σ is equal to the relative standard uncertainty $u_{\rm c}(r)$ of the measurement [34]. The area assigned to each individual measurement was chosen as proportional to the weight $1/u_{\rm c}^2(r)$. The ideogram for one cluster is then the sum of the Gaussian distributions for that cluster. Several different symbols in the ideogram of one carbon cluster represent measurements with different reference ions; the vertical dashed line is the weighted mean of all measurements for a given cluster.

These ideograms show that in all cases in which a sufficient number of measurements was performed, the distribution of the individual measurements is nearly Gaussian. The only exception is that of C_6 with only four data points. Furthermore, Figure 8 graphically shows that the distribution of the individual measurements for a given cluster and the deviations of the weighted means from the true values are all at the level of a few parts in 10^{-8}, as would be expected from the uncertainties, shown as error bars in the figure.

3.3.2 Mass-dependent systematic effect

Another way of representing the entire set of the cross-reference measurements is depicted in Figure 9. Here, the data points represent the weighted means of all individual measurements as a function of the mass difference $m - m_{\rm ref}$ between the two carbon clusters involved. The error bars are the uncertainties of the weighted means. As would be expected considering the enormous mass region that is spanned by these data, the figure shows the presence of a mass-dependent systematic effect. By use of a linear fit to the data, which by definition was constrained to pass through the origin, the magnitude of the effect was determined to be

$$\frac{\varepsilon_{\rm m}(r)}{r} = -1.6(4) \times 10^{-10}/\text{u} \times (m - m_{\rm ref})\,. \qquad (11)$$

A mass-dependent frequency ratio shift can be due to imperfections of the electric-quadrupole field or a misalignment of the precision trap's electrostatic trapping fields with respect to the magnetic-field axis [4,22]. The upper bound of the magnitude of these effects has previously been estimated [35] to be $|\varepsilon_{\rm m}(r)|/r = 2 \times 10^{-9}/\text{u} \times (m - m_{\rm ref})$.

Since the factors contributing to the mass-dependent effect are not completely controllable, it is believed that

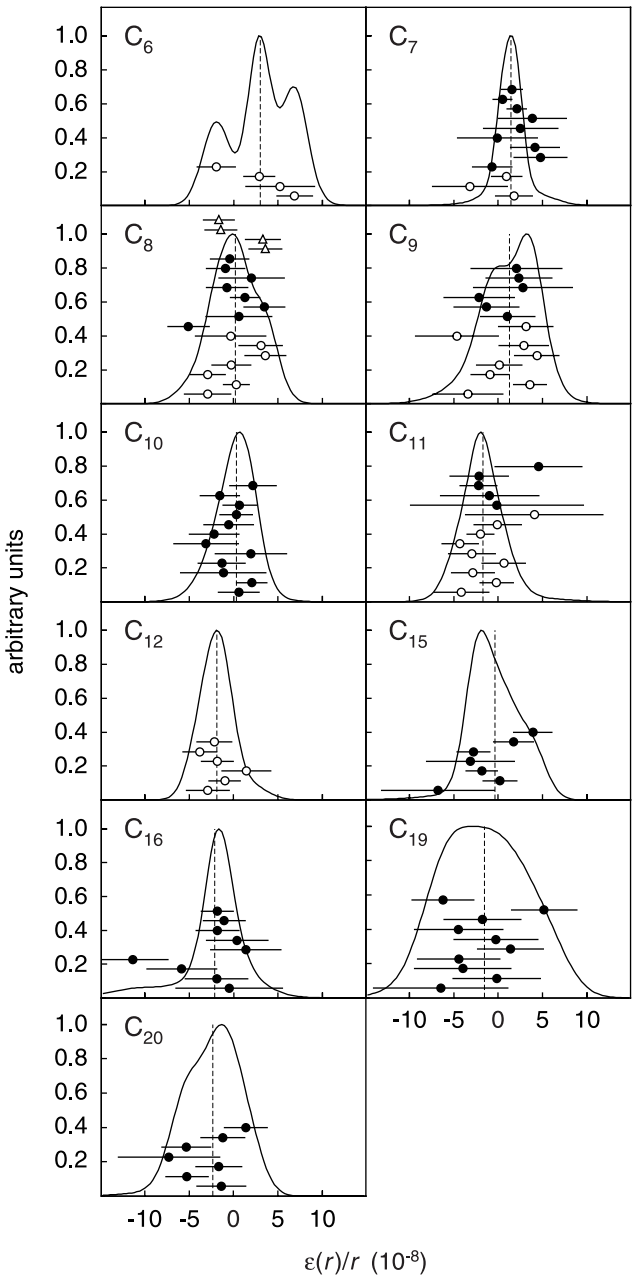

Fig. 8. Ideograms of all 114 cluster cross-reference measurements. The different symbols represent measurements with different reference ions: C_{10}^+ (empty circles), C_{12}^+ (filled circles), and C_{20}^+ (empty triangles).

its magnitude may change in future measurements due to small changes in electrostatic potentials or other trapping parameters. However, the magnitude of the effect did not appear to vary greatly, if at all, during the approximately three months which this study lasted. It was nevertheless decided not to correct for it in evaluating actual measurements, but instead to add a relative standard uncertainty which has the same magnitude:

$$\frac{u_{\mathrm{m}}(r)}{r} = 1.6 \times 10^{-10}/\mathrm{u} \times (m - m_{\mathrm{ref}})\,. \qquad (12)$$

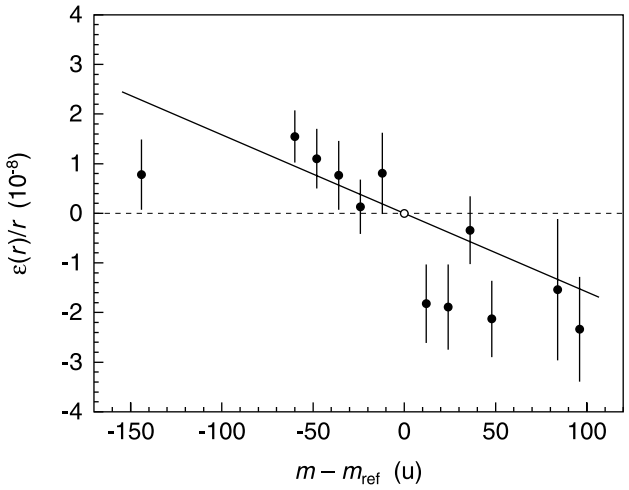

Fig. 9. Deviation of the weighted mean frequency ratios of all carbon cluster cross-reference measurements as a function of the mass difference $m - m_{\mathrm{ref}}$ between reference ion and ion of interest. The straight line is a linear least-squares fit to the data. The carbon cluster ions C_{10}^+, C_{12}^+, and C_{20}^+ were used as reference ions.

This equation shows the importance of choosing a reference ion whose mass is as close as possible to the mass of the ion of interest. In most past measurements, it was possible to keep $m - m_{\mathrm{ref}}$ below 20 u and thus the total relative effect below 5×10^{-9}.

3.3.3 Residual systematic uncertainty

At the time of the carbon cluster cross-reference measurements, the mass-dependent effect was clearly identified and its magnitude determined. The effect can therefore be corrected for, albeit only for this particular series of measurements. The result of this correction is shown in Figure 10. In this figure, the weighted means of all individual cross-reference measurements are shown as a function of the mass of the simulated ion of interest. The error bars represent the experimental uncertainties of the weighted means. Clearly, these results agree rather well with the true values, represented by the solid horizontal line.

The χ^2 of the experimental distribution of the cyclotron frequency ratios for each carbon cluster were then calculated according to the following formula:

$$\chi^2 = \sum_i \left[\frac{\varepsilon(r^i)}{u_{\mathrm{c}}(r^i)} \right]^2 , \qquad (13)$$

where $\varepsilon(r^i) = r^i - r_{\mathrm{th}}$ is the deviation of the measured frequency ratio from its known true value r_{th} and $u_{\mathrm{c}}(r^i)$ is the combined standard uncertainty of the individual frequency ratio.

After correction for the mass-dependent effect by use of equation (11), the reduced χ^2 of the distribution of the

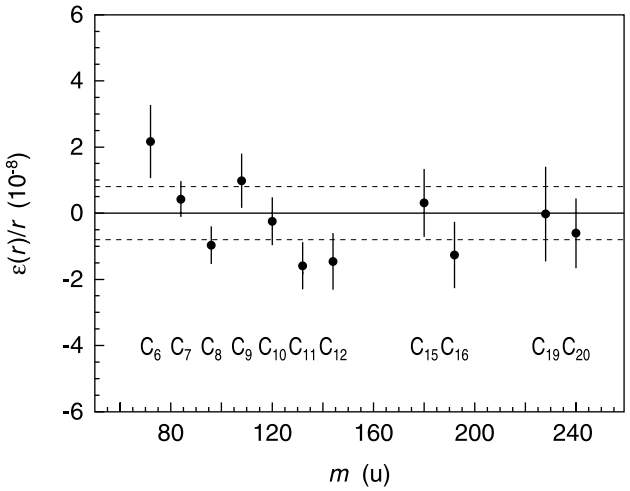

Fig. 10. Deviations of the weighted means of the cyclotron frequency ratios for all carbon cluster cross-reference measurements from their true value after correction for the mass-dependent effect by use of equation (11). The dashed lines indicate the residual systematic uncertainty that must be added to the uncertainties of the mean values in order to obtain a reduced χ^2 that obeys the condition $\chi^2/N \leq 1$.

individual frequency ratios about their true values[3] for all 114 cross-reference measurements shown in Figure 8 is $\chi^2/N = 0.96$. This indicates that the relative standard uncertainty $u_B(\nu_{\rm ref})/\nu_{\rm ref}$ due to the magnetic-field fluctuations was correctly determined and taken into account.

If for the individual data contributing to the mass value of one cluster size the weighted means are calculated as plotted in Figure 10, it becomes obvious that an additional systematic effect is still present. The reduced χ^2 of the distribution of the mean frequency ratios for all eleven carbon cluster species was therefore calculated and found to be $\chi^2/N = 2.02$. The fact that the reduced χ^2 is considerably greater than 1 confirms the presence of a residual systematic effect. Its magnitude can be determined from the condition $\chi^2/N \leq 1$ to be

$$\frac{u_{\rm res}(r)}{r} = 8 \times 10^{-9}\,. \qquad (14)$$

This uncertainty also constitutes the limit of mass accuracy of the ISOLTRAP experiment because all other uncertainties, being statistical in nature, can be reduced by an increased number of repeated measurements. This new limit is more than an order of magnitude smaller than the systematic uncertainty previously added to the final results.

4 Conclusions and outlook

A detailed study of the various contributions to the uncertainty of a measurement with the ISOLTRAP mass spectrometer was conducted. Several distinct effects were identified and their magnitudes measured where possible.

A technique was developed that allows an estimate of the uncertainty of a cyclotron frequency determination in the presence of contaminant ions in the precision trap. The contributions of random magnetic-field fluctuations to the uncertainty of a cyclotron frequency measurement were determined. These fluctuations were found to contribute a relative uncertainty which is directly proportional to the total measurement time for one cyclotron frequency ratio.

Carbon clusters $^{12}C_n$ ($6 \leq n \leq 20$) were used to quantify systematic effects in the mass measurement procedure with the ISOLTRAP apparatus. A mass-dependent systematic shift was identified and its magnitude found to be $-1.6(4) \times 10^{-10}/\mathrm{u} \times (m - m_{\rm ref})$. The residual systematic uncertainty after correction for the mass-dependent effect was determined to be $u_{\rm res}(r)/r = 8 \times 10^{-9}$, which also represents the present limit of mass accuracy of the ISOLTRAP system.

Based on the results of these measurements, modifications to the measurement procedure as well as a new evaluation procedure, which is described in detail in the Appendix, were defined. After these procedural changes, the limit of mass accuracy in ISOLTRAP measurements is more than a factor of 10 smaller than the systematic uncertainty previously added to the final results and about a factor of 4 smaller than the former best-case estimate [35]. In recent measurements, overall mass uncertainties of close to 10^{-8} have been reached for the first time in the case of the radioactive nuclide ^{74}Kr [36,37]. In the mass region below that covered by the carbon cluster cross-reference data, our recent mass measurements of the stable argon isotopes ^{36}Ar and ^{38}Ar [36] are in excellent agreement with other experimental data [31,38], indicating that the conclusions from the carbon cluster results can be extended to lower masses.

Investigations of the efficiency of cluster ion production with the matrix-assisted laser desorption and ionization time-of-flight (MALDI-TOF) apparatus at Mainz indicate that the commercial material Sigradur® may be better suited for the production of carbon clusters C_n, $n \leq 20$ [39]. Sigradur® is a material with ceramic properties that consists of pure carbon. It is obtained by thermal decomposition of a synthetic resin. Using this material, the present study could easily be extended to the lighter clusters C_n, $n \leq 5$.

In the future, it will be possible to perform absolute mass measurements of radioactive nuclides using carbon clusters as reference ions. As an added benefit, the masses of these clusters are evenly spaced at intervals of 12 u throughout the entire chart of the nuclides such that the maximal mass difference $m - m_{\rm ref}$ will be 6 u. As a consequence, the relative mass-dependent shift will be smaller than 1×10^{-9} in future high-precision mass measurements.

This study has also made apparent some weaknesses in the experimental setup and measurement procedure. An improved vacuum in the precision trap may reduce the amount of contamination created by charge exchange reactions and would allow even longer observation times,

[3] For the calculation of the reduced χ^2, the relation χ^2/N was used since in equation (13) no degree of freedom was lost in the calculation of a mean value.

such as are needed to resolve contaminations by isomers with excitation energies smaller than 100 keV. A stabilization of the gaseous-helium pressure in the magnet cryostat and of the temperature in the warm bore of the magnet hold the prospect of greatly reducing the observed magnetic-field fluctuations. Finally, a modified measurement cycle in which reference ion and ion of interest are observed alternatingly in quick succession will effectively eliminate the effect of any remaining such fluctuations. Improvements of the setup that address these issues are currently being studied.

The authors wish to thank Georges Audi (CSNSM Orsay) for valuable discussions and advice concerning the evaluation and interpretation of the present study. The support by the European Commission within the EUROTRAPS network under contract number FMRX-CT-97-0144 as well as within the NIPNET network under contract number HPRI-CT-2001-50034 and the support of the German Ministry for Education and Research (BMBF) are gratefully acknowledged.

Appendix A: Evaluation procedure

A.1 Individual cyclotron frequencies of the ion of interest

For all TOF resonances recorded with ions that are potentially subject to contamination, *i.e.* all ions delivered by ISOLDE, the cyclotron frequencies are determined using a count rate class analysis. The cyclotron frequencies ν^i of the individual measurements and their uncertainties $u(\nu^i)$ are determined according to the procedure described in Section 3.1.2.

A.2 Individual cyclotron frequencies of the reference ion

For each TOF resonance of the ion of interest recorded at time t_1, the cyclotron frequency of the reference ion is determined from the two references just before and just after it (times t_0 and t_2). All times are understood to mean the center of the interval between the beginning and the end of a TOF resonance measurement. Using the least-squares method, the cyclotron frequency of the two measurements are interpolated to t_1, yielding the cyclotron frequency ν_{ref} of the reference ion.

The combined relative standard uncertainty of the cyclotron frequency of the reference ion at time t_1 is found by quadratically adding the experimental relative standard deviation found in this way and the relative standard uncertainty due to the fluctuation of the magnetic field $u_B(\nu^i_{\mathrm{ref}})/\nu^i_{\mathrm{ref}}$ which is calculated according to equation (10):

$$\frac{u_{\mathrm{c}}(\nu^i_{\mathrm{ref}})}{\nu^i_{\mathrm{ref}}} = \sqrt{\left[\frac{s(\nu^i_{\mathrm{ref}})}{\nu^i_{\mathrm{ref}}}\right]^2 + \left[\frac{u_B(\nu^i_{\mathrm{ref}})}{\nu^i_{\mathrm{ref}}}\right]^2}\,. \tag{15}$$

A.3 Cyclotron frequency ratios

For all individual measurements of a given ion species, the cyclotron frequency ratios r^i and their combined relative uncertainties $u_{\mathrm{c}}(r^i)/r^i$ are calculated according to

$$r^i = \frac{\nu^i_{\mathrm{ref}}}{\nu^i} \tag{16}$$

and

$$\frac{u_{\mathrm{c}}(r^i)}{r^i} = \sqrt{\left[\frac{s(\nu^i)}{\nu^i}\right]^2 + \left[\frac{u_{\mathrm{c}}(\nu^i_{\mathrm{ref}})}{\nu^i_{\mathrm{ref}}}\right]^2}\,. \tag{17}$$

In the case that two or more measurements of one species of ions were made during the same on-line experiment, the weighted mean $\bar{r}$ of the frequency ratio and its relative standard uncertainty $u(\bar{r})/\bar{r}$ are calculated:

$$\bar{r} = \frac{\sum_i \frac{r^i}{u^2_{\mathrm{c}}(r^i)}}{\sum_i \frac{1}{u^2_{\mathrm{c}}(r^i)}} \tag{18}$$

and

$$\frac{u(\bar{r})}{\bar{r}} = \frac{1}{\bar{r}} \frac{1}{\sqrt{\sum_i \frac{1}{u^2_{\mathrm{c}}(r^i)}}}\,. \tag{19}$$

Finally, the combined relative standard uncertainty of the mean frequency ratio is found by adding to the relative standard uncertainty calculated by use of equation (19) the relative uncertainty due to the mass-dependent systematic effect $u_{\mathrm{m}}(\bar{r})/\bar{r}$ and the residual relative uncertainty $u_{\mathrm{res}}(\bar{r}/\bar{r})$:

$$\frac{u_{\mathrm{c}}(\bar{r})}{\bar{r}} = \sqrt{\left[\frac{u(\bar{r})}{\bar{r}}\right]^2 + \left[\frac{u_{\mathrm{m}}(\bar{r})}{\bar{r}}\right]^2 + \left[\frac{u_{\mathrm{res}}(\bar{r})}{\bar{r}}\right]^2}\,, \tag{20}$$

where $u_{\mathrm{m}}(\bar{r})/\bar{r}$ is calculated according to equation (12) and $u_{\mathrm{res}}(\bar{r})/\bar{r}$ is given by equation (14).

References

1. E. Kugler, Hyp. Interact. **129**, 23 (2000)
2. G. Bollen, Nucl. Phys. A **693**, 3 (2001)
3. F. Herfurth *et al.*, Nucl. Instrum. Meth. A **469**, 254 (2001)
4. G. Bollen *et al.*, Nucl. Instrum. Meth. A **368**, 675 (1996)
5. G. Gräff, H. Kalinowsky, J. Traut, Z. Phys. A **297**, 35 (1980)
6. G. Bollen *et al.*, J. Appl. Phys. **68**, 4355 (1990)
7. D.L. Farnham *et al.*, Phys. Rev. Lett. **75**, 3598 (1995)
8. G. Gabrielse *et al.*, Phys. Rev. Lett. **82**, 3198 (1999)
9. S. Brunner *et al.*, Eur. Phys. J. D **15**, 181 (2001)
10. T. Fritioff *et al.*, Eur. Phys. J. D **15**, 141 (2001)
11. M.P. Bradley *et al.*, Phys. Rev. Lett. **83**, 4510 (1999)
12. J.C. Hardy, I.S. Towner, Hyp. Interact. **132**, 115 (2001)
13. H.W. Kroto *et al.*, Nature **318**, 162 (1985)
14. W. Krätschmer *et al.*, Nature **347**, 354 (1990)
15. H.W. Kroto, Int. J. Mass Spectrom. Ion Proc. **200**, 253 (2000)

16. C. Lifshitz, Int. J. Mass Spectrom. Ion Proc. **200**, 423 (2000)
17. K. Blaum *et al.*, Eur. Phys. J. A (2002), in press
18. A. Kellerbauer *et al.*, Hyp. Int. (2002), submitted
19. T.J. Quinn, I.M. Mills, *The International System of Units (SI)*, 7th edn. (Bureau International des Poids et Mesures, Sèvres, France, 1998)
20. C. Scheidenberger *et al.*, Nucl. Phys. A **701**, 574c (2002)
21. P. Wurz, K.R. Lykke, Chem. Phys. **184**, 335 (1994)
22. L.S. Brown, G. Gabrielse, Rev. Mod. Phys. **58**, 233 (1986)
23. G. Savard *et al.*, Phys. Lett. A **158**, 247 (1991)
24. M. König *et al.*, Int. J. Mass Spectrom. Ion Proc. **142**, 95 (1995)
25. G. Bollen *et al.*, Phys. Rev. C **46**, R2140 (1992)
26. J. Oberheide, P. Wilhelms, M. Zimmer, Meas. Sci. Technol. **8**, 351 (1997)
27. P.W. Anderson, Phys. Rev. Lett. **9**, 309 (1962)
28. P.W. Anderson, Y.B. Kim, Rev. Mod. Phys. **39**, 39 (1964)
29. J.B. Ketterson, S.N. Song, *Superconductivity* (Cambridge University Press, Cambridge, 1999)
30. R.S. van Dyck Jr, D.L. Farnham, P.B. Schwinberg, J. Mod. Opt. **39**, 243 (1992)
31. I. Bergström *et al.*, Nucl. Instrum. Meth. A **487**, 618 (2002)
32. B.R. Eggen, R.L. Johnston, J.N. Murrell, J. Chem. Soc. Farad. Trans. **90**, 3029 (1994)
33. F.R. Manby, R.L. Johnston, C. Roberts, Commun. Math. Comp. Chem. **38**, 111 (2001)
34. M. Aguilar-Benitez *et al.*, Phys. Lett. B **170**, 1 (1986)
35. D. Beck *et al.*, Nucl. Instrum. Meth. B **126**, 374 (1997)
36. F. Herfurth *et al.*, Eur. Phys. J. A (2002), in press
37. A. Kellerbauer, Ph.D. thesis, University of Heidelberg, 2002, `http://www.ub.uni-heidelberg.de/archiv/2463`
38. G. Audi, A.H. Wapstra, Nucl. Phys. A **595**, 409 (1995)
39. K. Blaum *et al.*, Eur. Phys. J. D (2002), to be published